applied sciences

MDPI

Article

Experimental Research on the Influence of Repeated Overheating on the Thermal Diffusivity of the Inconel 718 Alloy

Elisabeta Roxana Ungureanu Arva [1,2], Marioara Abrudeanu [1,3], Denis Aurelian Negrea [4,*], Andrei Galatanu [5], Magdalena Galatanu [5], Alin-Daniel Rizea [6], Daniel-Constantin Anghel [6], Mihai Branzei [3,7], Alexandra Ion Jinga [1,8] and Mircea Ionut Petrescu [7]

1 Doctoral School of Materials Science and Engineering, National University of Science and Technology POLITEHNICA Bucharest, Splaiul Independenţei nr. 313, District 6, 060042 Bucharest, Romania; elisabetaroxanaungureanu@gmail.com (E.R.U.A.); abrudeanu@gmail.com (M.A.); alexandra.jinga@nuclear.ro (A.I.J.)
2 Nuclear Fuel Plant, Campului Street, nr. 1, 115400 Mioveni, Romania
3 Technical Sciences Academy of Romania, Calea Victoriei, nr. 118, District 1, 010093 Bucharest, Romania; mihai.branzei@upb.ro
4 Regional Center of Research & Development for Materials, Processes and Innovative Products Dedicated to the Automotive Industry (CRC&D-AUTO), National University of Science and Technology POLITEHNICA Bucharest, University Center Pitesti, Str. Targu din Vale, Nr. 1, 110040 Pitesti, Romania
5 National Institute of Materials Physics, Atomistilor 405A, 077125 Magurele, Romania; gala@infim.ro (A.G.); magdalena.galatanu@infim.ro (M.G.)
6 Department of Manufacturing and Industrial Management, National University of Science and Technology POLITEHNICA Bucharest, University Center Pitesti, Street Târgul din Vale, nr. 1, 22, 110040 Pitesti, Romania; alin_daniel.rizea@upb.ro (A.-D.R.); dc.anghel@upb.ro (D.-C.A.)
7 Department of Engineering and Management of Metallic Materials Casting, Faculty of Materials Science and Engineering, National University of Science and Technology POLITEHNICA Bucharest, Splaiul Independenţei nr. 313, District 6, 060042 Bucharest, Romania; ipetrescu@yahoo.com
8 Institute for Nuclear Research, Campului Street, nr. 1, 115400 Mioveni, Romania
* Correspondence: aurelian.negrea@upb.ro

check for updates

Citation: Arva, E.R.U.; Abrudeanu, M.; Negrea, D.A.; Galatanu, A.; Galatanu, M.; Rizea, A.-D.; Anghel, D.-C.; Branzei, M.; Jinga, A.I.; Petrescu, M.I. Experimental Research on the Influence of Repeated Overheating on the Thermal Diffusivity of the Inconel 718 Alloy. *Appl. Sci.* **2024**, *14*, 8574. https://doi.org/10.3390/app14188574

Academic Editor: Chiara Soffritti

Received: 19 August 2024
Revised: 13 September 2024
Accepted: 17 September 2024
Published: 23 September 2024

Abstract: The Inconel 718 superalloy, a precipitation-hardenable material, is of particular interest for applications involving components operating under extreme conditions due to its excellent mechanical properties, high corrosion resistance at temperatures up to 700 °C, and good workability. At high temperatures, thermal transfer processes are crucial for temperature distribution across the component's section, structural transformations, and variations in the alloy's properties. The history of accidental overheating events is critical for the microstructure and properties of the alloy. Studies on thermal transfer in the Inconel 718 alloy available in the literature typically focus on the alloy in its as-delivered state. The experimental research presented in this paper examines the influence of repeated overheating history on the thermal diffusivity of the alloy.

Keywords: Inconel; overheating; solar energy; microstructural transformations; thermal transfer

1. Introduction

Inconel 718 belongs to the category of nickel-based superalloys and is known for its tensile, fatigue, creep, and fracture characteristics, as well as its excellent corrosion resistance at temperatures above 650 °C—properties superior to stainless steels. These characteristics, combined with good welding properties, resistance to post-weld cracking, and good processing properties, justify its use in difficult operating conditions: sheet metal parts for aircraft and gas turbine engines, components in oil refineries, cooling equipment for seawater, cryogenic tanks, and other uses where heat transfer processes are important [1–4]. Inconel 718 exhibits excellent corrosion resistance at high temperatures due to its high contents of nickel and chromium. This alloy falls under the category of precipitation-hardened nickel-based superalloys, and its good mechanical properties result

from both solid solution hardening and precipitation hardening processes. To enhance its mechanical characteristics, this alloy includes elements such as aluminum, titanium, niobium, molybdenum, and tungsten [5–8]. Solid solution hardening occurs when alloying elements dissolve into the base metal matrix, forming a solid solution with improved strength. The most critical hardening mechanism is the precipitation of intermetallic phases from the solid solution [9–22]. The chemical composition of the alloy and the applied heat treatment determine the nature, distribution, and morphology of the formed precipitates. The elements that contribute to precipitation hardening are primarily Nb, Al, and Ti. Heat treatment involves solution quenching at temperatures between 970 °C and 1175 °C, followed by one or more tempering steps at temperatures between 600 °C and 815 °C. During cooling, aluminum and titanium, which are supersaturated in the γ solid solution at the treatment temperature, precipitate to form the γ' phase with the stoichiometric formula Ni_3(Al, Ti). Niobium is the primary hardening element in the alloy, forming the γ'' compound (Ni_3Nb) by precipitation. Grain boundary hardening occurs through the precipitation of carbides. The formation of discrete globular carbides along the grain boundaries prevents their migration, thereby enhancing creep resistance and maintaining sufficient ductility in the surrounding matrix. This ductility allows the matrix to absorb the resulting stresses, preventing premature fracture. However, if carbides precipitate as a continuous film along the grain boundaries, the properties of the alloy decrease significantly. The grain size, as well as the size, morphology, and distribution of the precipitates, plays a crucial role in determining the alloy's behavior in various applications [5,23–25].

Thermal diffusivity plays a crucial role in determining the performance of Inconel 718 under high-temperature operating conditions. It influences the cooling rate during heat treatments, as well as the size and distribution of precipitated particles. Depending on the cooling rate, either fine microstructures with good mechanical properties or brittle phases with low material durability can be obtained. High thermal diffusivity enhances the material's ability to dissipate heat, which is vital in high-temperature applications, preventing overheating and material degradation. Thermal diffusivity also impacts oxidation at elevated temperatures. An alloy with adequate thermal diffusivity can form a uniform protective oxide layer, improving corrosion resistance in oxidizing environments. Uniform heat distribution helps prevent the formation of cracks and other surface defects, thereby maintaining the structural integrity of the material under severe operating conditions. Adequate thermal diffusivity ensures a stable microstructure, optimal mechanical strength, efficient thermal conductivity, and increased corrosion resistance. Controlling this property through manufacturing and heat treatment processes is essential for maximizing the performance of this superalloy in critical applications.

Studies in the literature on the influence of overheating on the microstructure and thermal diffusivity of nickel-based superalloys, particularly Inconel 718, have focused on the alloy in its as-delivered state, the role of alloying elements in enhancing thermal diffusivity, the modeling of thermal properties and thermally induced stresses, and the determination of the variation in diffusivity at measurement temperatures up to 700–1000 °C [26–37].

The experimental research presented in this paper examines the influence of cyclic overheating on the variation in thermal diffusivity in Inconel 718, consistently comparing it to the diffusivity of the material in its as-delivered (standard) state.

2. Materials and Experimental Techniques

The Inconel 718 alloy, plastically deformed, used for thermal shock testing, has the following composition: 52.16% Ni, 17.05% Fe, 16.76% Cr, 2.96% Mo, 5.36% Nb, 0.23% Mn, 0.17% Si, 1.12% Ti, and 0.42% Co. The characteristics of the Inconel 718 alloy are given by ASTM B637 N07718 "Standard Specification for Nickel Alloy Bars, Forgings, and Forging Stock for Moderate or High Temperature Service" [38]. The microstructure revealed intergranular lamellar precipitates distributed relatively uniformly at the grain boundaries (Figure 1b,f), the presence of large polyhedral precipitates/particles inside

the grains (Figure 1a,c,d), and the presence of some structures with rectangular geometric development (Figure 1e).

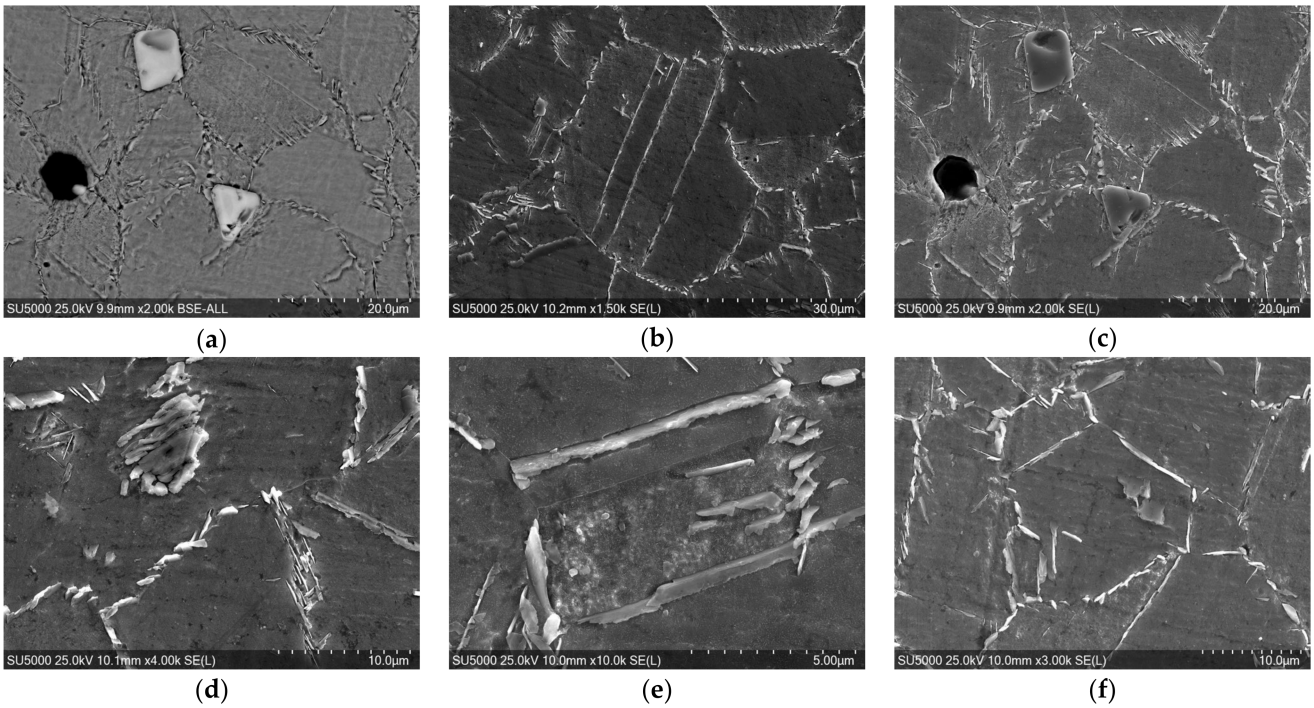

Figure 1. The SEM microstructures for the alloy as delivered, containing large polyhedral precipitates/particles inside the grains (**a**,**c**,**d**), intergranular lamellar precipitates at the grain boundaries (**b**,**f**) and structures with rectangular geometric development (**e**).

Cyclic overheating at high temperatures was simulated by thermal shocks using solar energy. The specimens for thermal shock testing have a parallelepipedal shape with a square base of 7 mm sides and 10 mm height.

The height of the sample is oriented according to the deformation direction of the alloy. The surface of the samples was mechanically polished using 800-grit abrasive paper. The shocks were applied to the upper base of the parallelepipedal sample positioned vertically. Thermal shock testing was carried out in the Solar Furnace at the PROMES laboratory, Font Romeu-Odeillo, France (Figure 2). Cyclic thermal shocks were used in the temperature range of 700–1000 °C with a constant temperature duration of each cycle of 30 s.

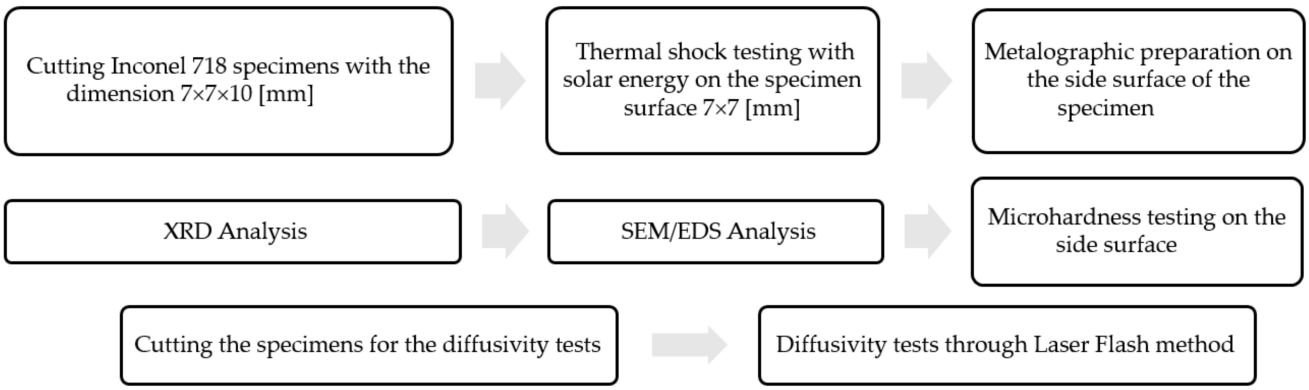

(**A**)

Figure 2. *Cont.*

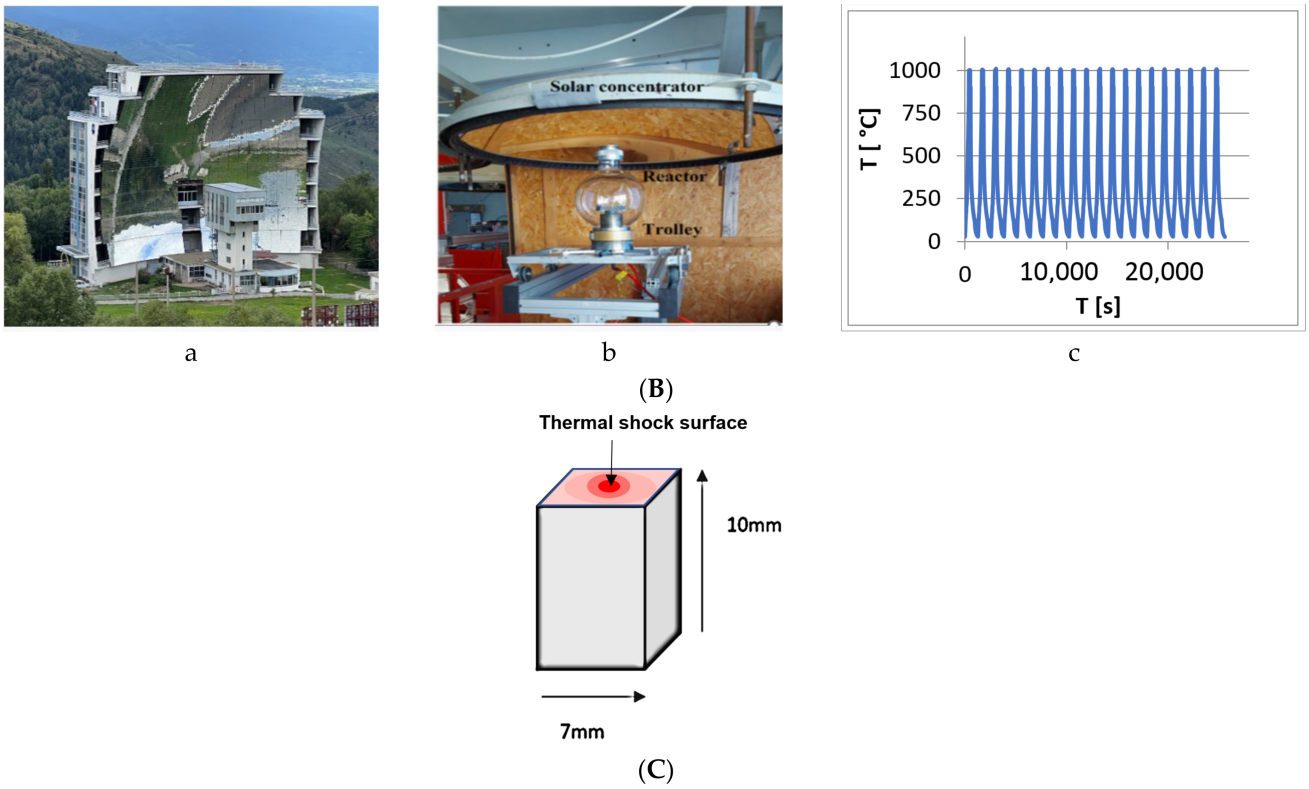

Figure 2. (**A**) Diagram for conducting experimental research. (**B**) Testing samples in solar furnace: a—image of solar furnace, PROMES laboratory; b—test facility; c—treatment cycle for 20 thermal shock cycles at 1000 °C. (**C**) Specimen geometry and positioning.

The thermal transport properties were investigated using a Laser Flash Analyzer model Netzsch LFA 457 Microflash (NETZSCH-Gerätebau GmbH, München, Germany) from room temperature up to 1050 °C. The microhardness measurements were carried out with FALCON equipment, series 500 (INNOVATEST Europe, Maastricht, The Netherlands). For microscopic analysis, samples were prepared by mechanical grinding and etched with Adler's reagent. The characterization by SEM-EDS was carried out using a HITACHI SU5000 electron microscope (Hitachi High-Tech Corporation, Tokyo, Japan) equipped with a backscattered electron detector and an energy-dispersive fluorescence spectroscopy module for elemental analysis.

3. Experimental Results

3.1. Microstructural and Elemental Chemical Characterization of Samples Subjected to Cyclic Thermal Shocks

The SEM analysis of the samples treated at 700 °C revealed large, rounded, light-colored precipitates (Figure 3a) and dark-colored intergranular precipitates (Figure 3b) with distributions similar to the grain boundaries of the initial interdendritic structure (Figure 3c).

Dark intergranular precipitates contain Nb, Al, and Mo. In these areas, the presence of Si and C is also noticeable (Figure 4).

Large light-colored precipitates with rounded shapes contain niobium, molybdenum, and titanium, with small percentages of silicon, carbon, and aluminum (Figure 5). The large intragranular precipitates contain Nb, Ti, and Mo. The presence of Nb and titanium was explained by sandwich structures of type $\gamma''/\gamma'/\gamma''$, resulting from the formation of the γ'' phase on existing γ' structures. The high participation of molybdenum in these precipitates is noted in the literature. The intragranular precipitates are rich in C, Nb, Mo, Ti, carbides and fine precipitates of γ' [29,30].

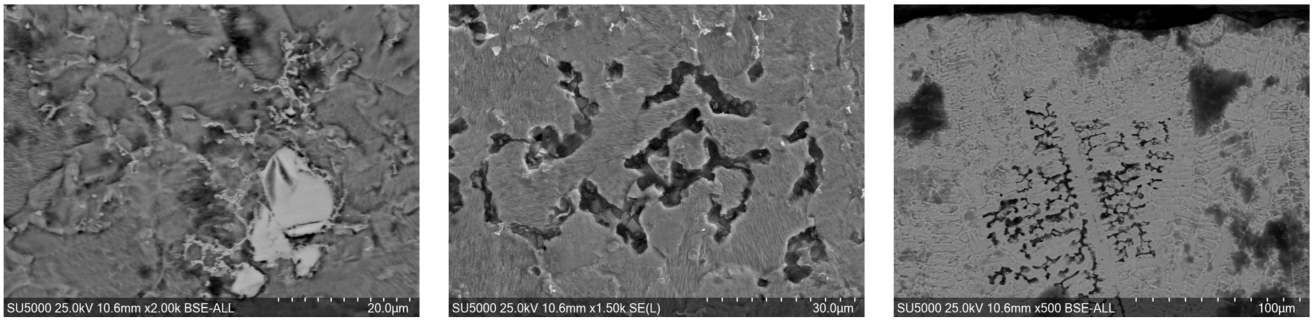

(**a**) (**b**) (**c**)

Figure 3. The microstructure of the sample treated at 700 °C, 3 cycles consisting of: large, rounded, light-colored precipitates (**a**), dark-colored intergranular precipitates (**b**) and interdendritic structure (**c**).

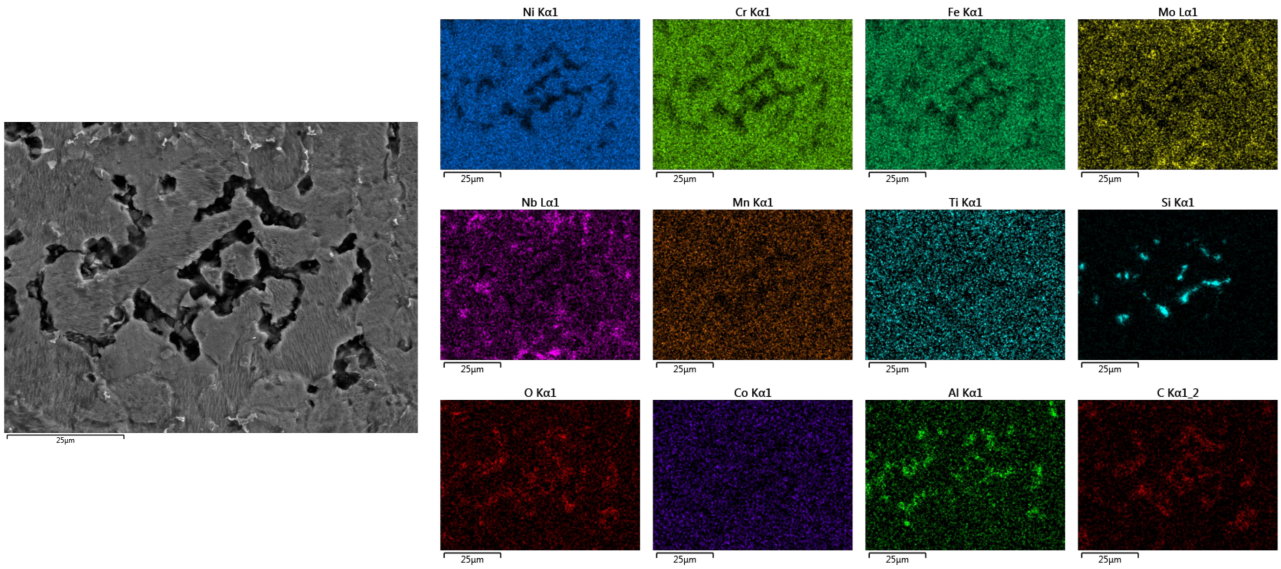

Figure 4. Chemical elemental composition mapping in an area with preferentially interdendritically arranged dark precipitates (700 °C, 3 cycles).

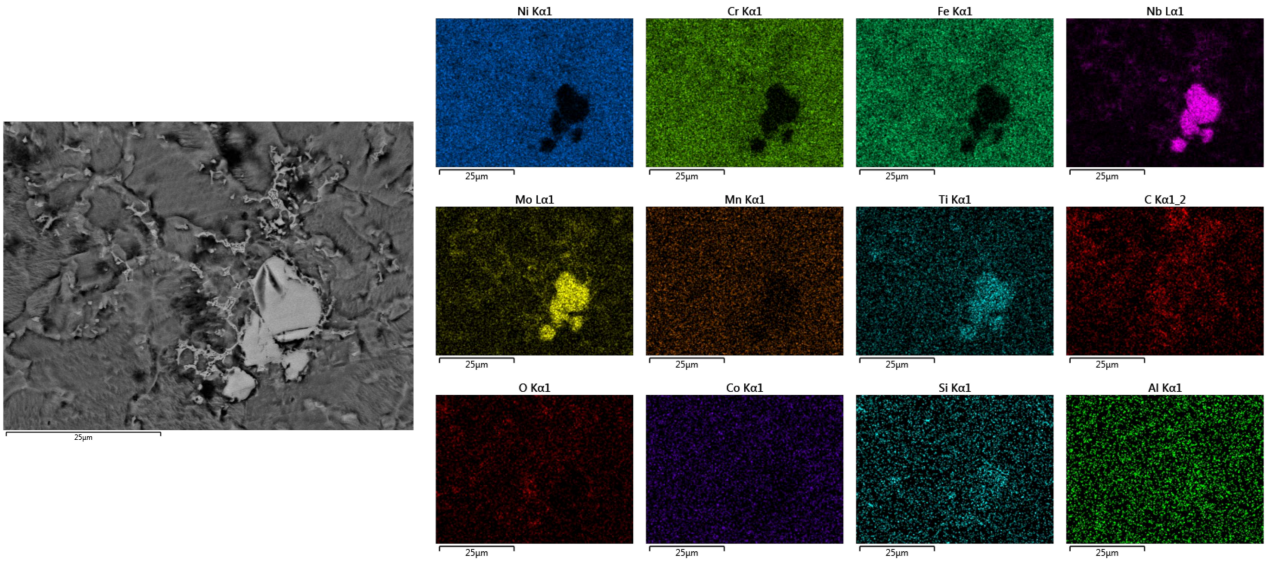

Figure 5. Chemical elemental composition mapping in high-precipitation area in light color of sample treated at 700 °C, 3 cycles.

A line-scan analysis of the sample cross-section (Figure 6) highlights the association of Mo-Nb in large intergranular precipitates and carbide presence. An increased number of thermal cycles (700 °C, 20 cycles) leads to the formation of large precipitates, rich in niobium, molybdenum, and titanium, arranged in rows oriented perpendicularly to the applied shock surface, as well as the development of a superficial oxidic layer (Figure 7).

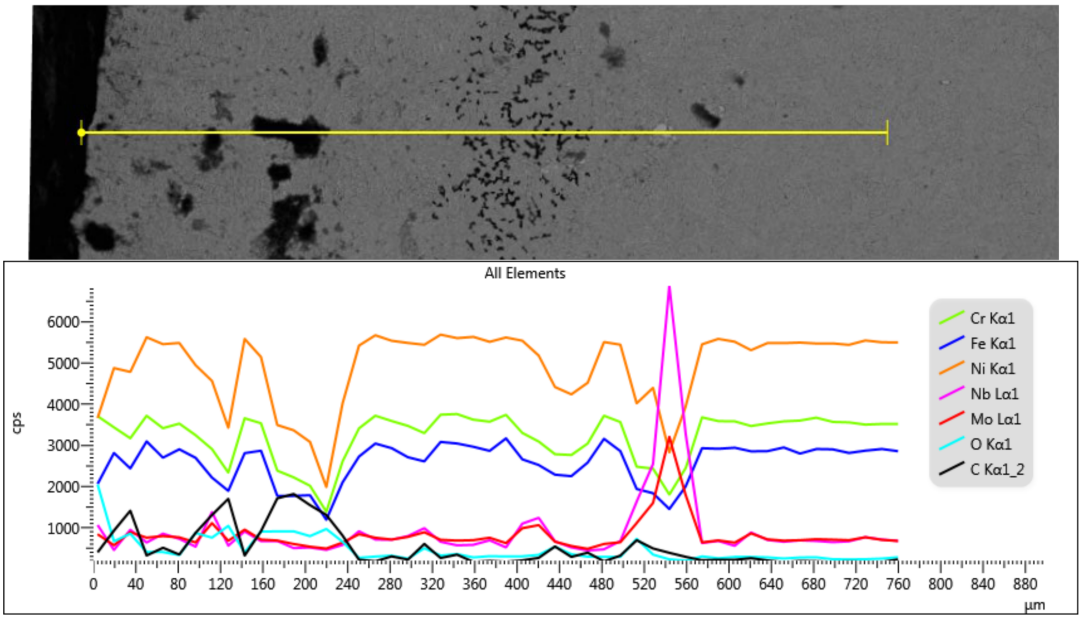

Figure 6. Cross-section line-scan analysis for the sample treated at 700 °C, 3 thermal cycles.

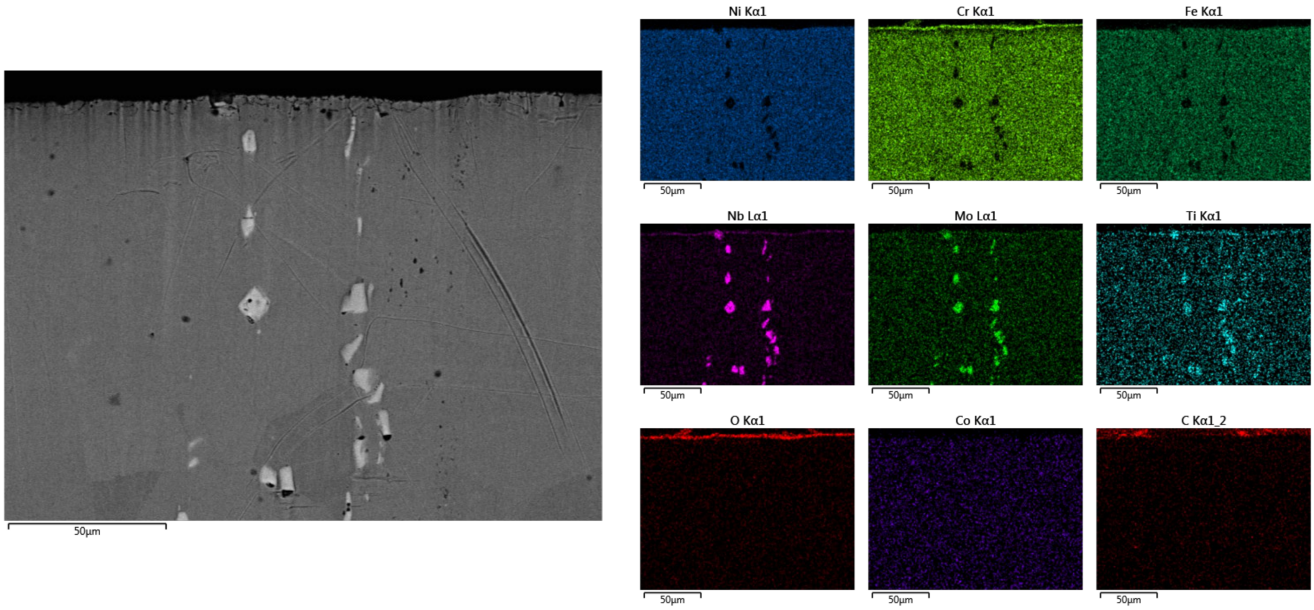

Figure 7. Chemical elemental composition mapping of sample treated at 700 °C for 20 cycles.

The increase in temperature causes the oxide layer to thicken, with the alloying elements showing a preferential distribution relative to the metal–oxide interface (Figure 8).

Regarding the influence of the thermal shock applied at 960 °C on the composition of the oxide layer formed on the Inconel 718 alloy, Shu-liang Wang [27] notes the presence of a protective film composed of Cr_2O_3 and $(Cr, Fe)_2O_3$ and the presence of hardening alloying elements (Ti and Nb) in the film—$Ti_{0.95}$ $Nb_{0.95}$ O_4. The compositions of these elements were also determined through XRD for alloys subjected to thermal shocks—results that were not

included in the present article. This paper provides an elemental chemical characterization across the entire thickness of the oxide layer.

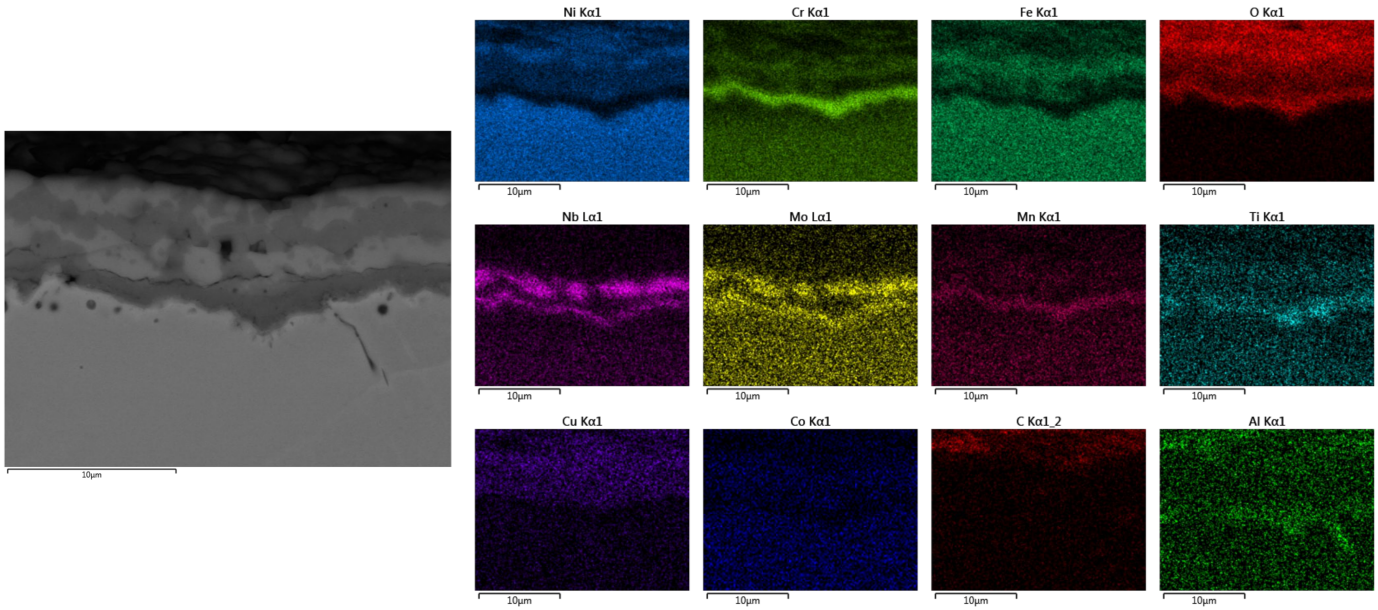

Figure 8. Chemical elemental composition mapping in the surface layer of the sample treated at 800 °C for 3 cycles.

At 800 °C, three cycles, the distribution of alloying elements in the oxide layer shows a continuous chromium-rich layer at the metal–oxide interface, reflecting the profile of the interface (Figures 8 and 9). This is followed outwardly by a layer rich in niobium, molybdenum, and titanium. Manganese is preferentially distributed in the chromium-rich layer, while aluminum is present throughout the thickness of the oxide layer (Figure 8).

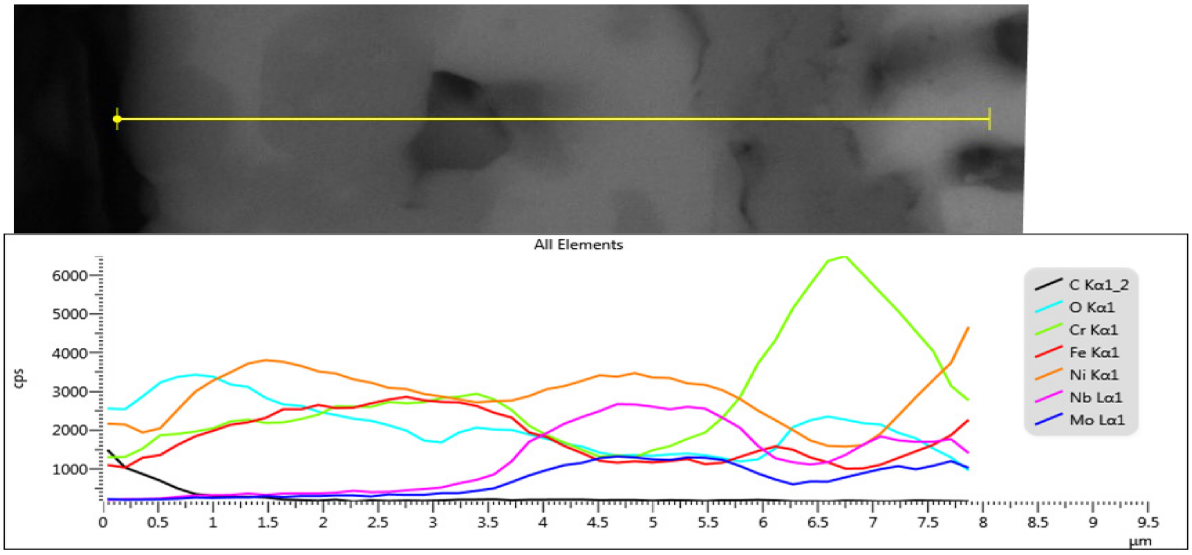

Figure 9. Line-scan analysis showing the distribution of elements in the surface layer of the sample treated at 800 °C for 3 cycles.

With an increased number of cycles (nine cycles at 800 °C), the structure consists of lamellar precipitates at the grain boundaries and coarse precipitates with rounded intergranular shapes (Figure 10). It is also observed that the light-colored, coarse intragranular precipitates contain up to 78.91% Nb (spectrum 3), while the intergranular lamellae contain less niobium (spectrum 2).

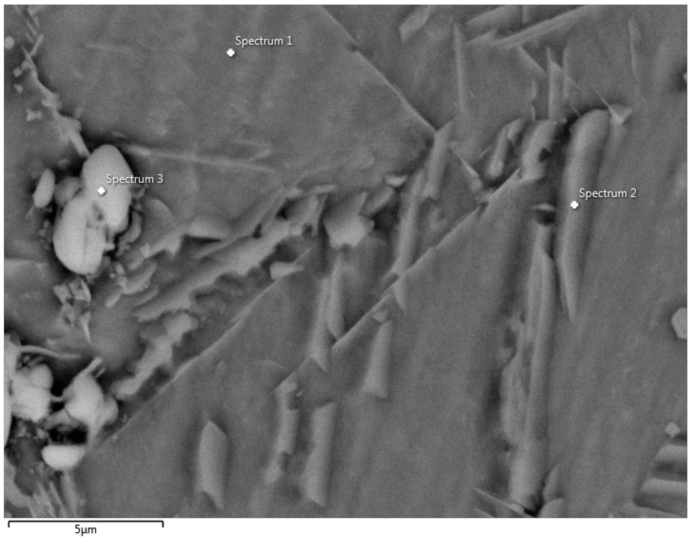

Spectrum Label	Spectrum 1	Spectrum 2	Spectrum 3
Al	0.68	0.61	0.08
Si	0.14	0.14	0.09
Ti	0.97	1.10	6.38
Cr	18.24	16.43	3.35
Mn	0.21	0.18	0.00
Fe	18.44	16.58	3.04
Co	0.44	0.40	0.07
Ni	51.74	51.85	7.50
Nb	5.55	9.46	78.91
Mo	3.60	3.24	0.57
Total	100.00	100.00	100.00

Figure 10. SEM-EDS analysis of sample treated at 800 °C for 9 cycles.

The gamma double-prime precipitate is stable only up to temperatures around 650–703 °C. Prolonged exposure to high temperatures leads to the formation of the delta phase, but the samples in the experimental program were not subjected to extended high-temperature treatments.

For shock temperatures above the tempering temperatures (900 °C and 1000 °C), the structure stabilizes, forming large light-colored precipitates arranged in strings oriented perpendicular to the shock surface. These precipitates are rich in niobium, molybdenum, and titanium (Figure 11).

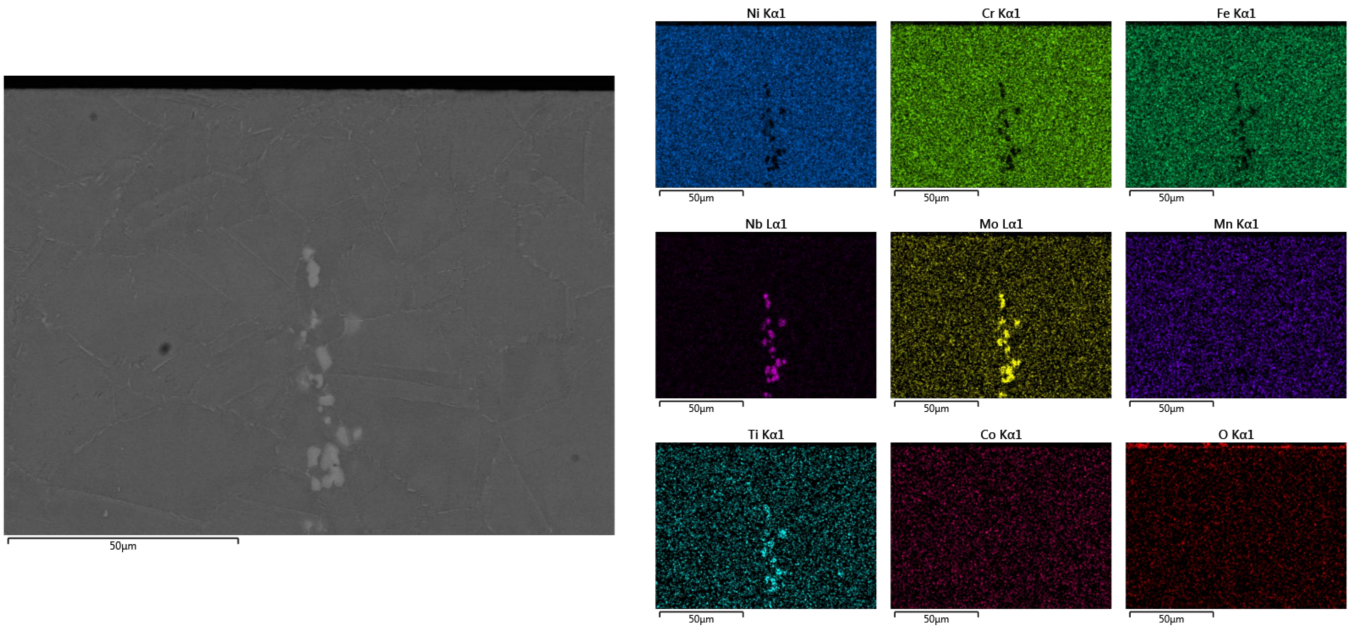

Figure 11. Chemical elemental composition mapping for the sample treated at 900 °C, 9 cycles.

The increase in temperature and the number of thermal cycles leads to a decrease in the number and an increase in the size of precipitates arranged in rows oriented perpendicular to the thermal shock surface (Figure 12).

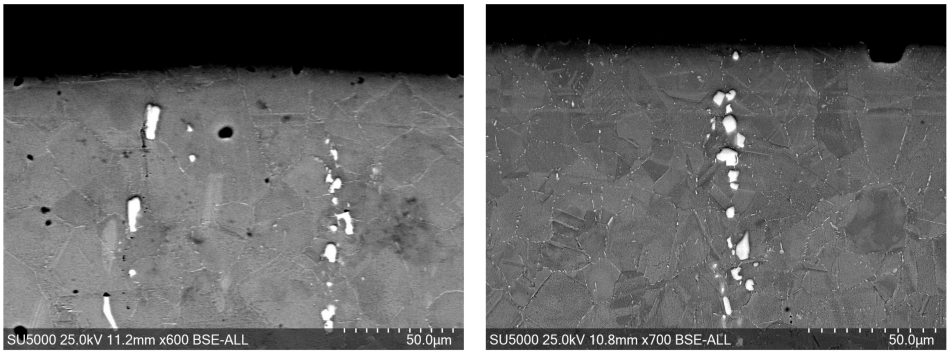

(**a**) (**b**)

Figure 12. Microstructures formed at 1000 °C for (**a**) 12 cycles and (**b**) 9 thermal shock cycles.

3.2. The Influence of Cyclic Shocks on Thermal Diffusivity

The variation in the thermal diffusivity of the samples treated at temperatures ranging from 700 °C to 1000 °C, with 3 to 20 cycles of thermal shocks, was determined over a range of 20 °C to 1000 °C. The thermal diffusivity of the samples was analyzed from two perspectives: the influence of thermal shock temperature for the same number of applied shocks and the influence of the number of applied shocks at the same thermal shock temperature. The diffusivity variation curves were compared to the diffusivity of the as-delivered reference material.

3.2.1. The Influence of Shock Application Temperature for the Same Number of Shock Cycles

Previous studies on the microstructural changes induced in the Inconel 718 alloy through cyclic thermal stresses, performed at low heating/cooling rates [27,28], have highlighted diffusion processes. These processes are much less evident for samples subjected to thermal shocks generated by solar energy.

The variation in the thermal diffusivity of the standard sample with measurement temperature shows a significant maximum at 700 °C and an inflection point at approximately 820 °C (Figure 13). A similar maximum was also observed by Hazotte and Archambault at 750 °C [33]. This variation can be explained by structural transformations that occur during the heat treatment.

The variation in thermal diffusivity with shock temperature indicates that for the same number of shocks, the values are quite close and remain below those of the standard sample, with small maxima around 700 °C, within the range of 600 °C to 800 °C (Figure 13).

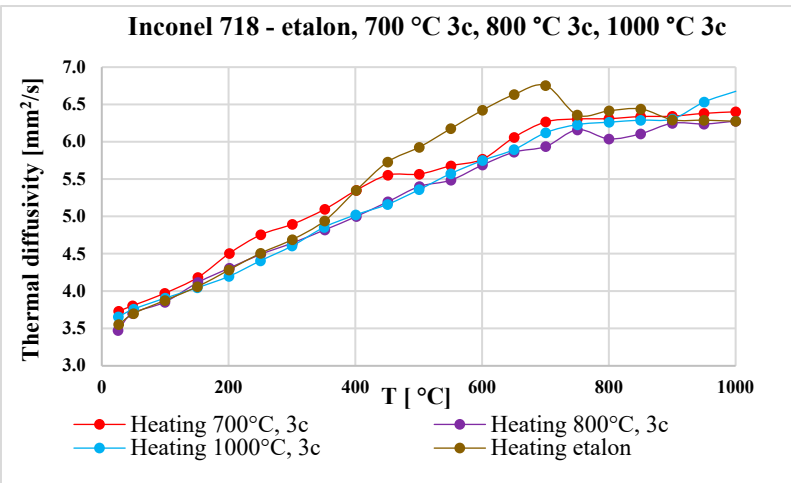

(**a**)

Figure 13. *Cont.*

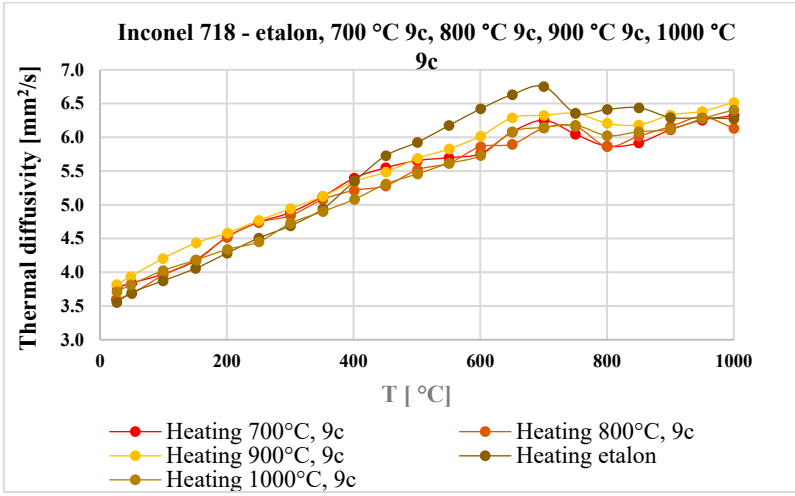

(**b**)

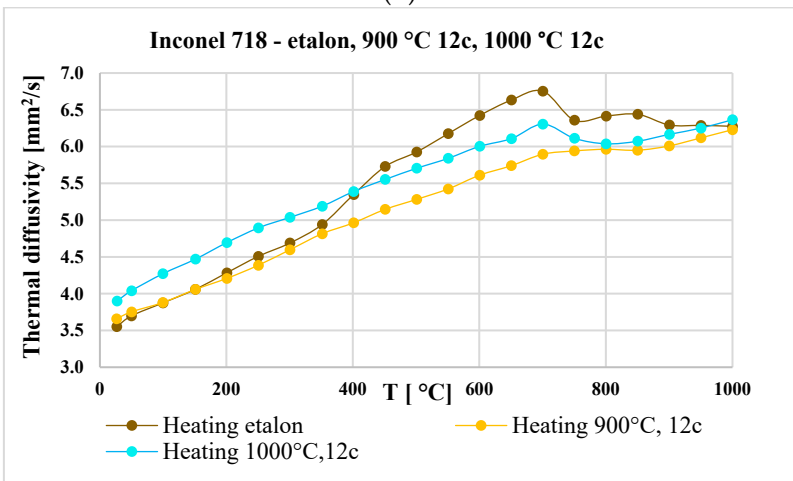

(**c**)

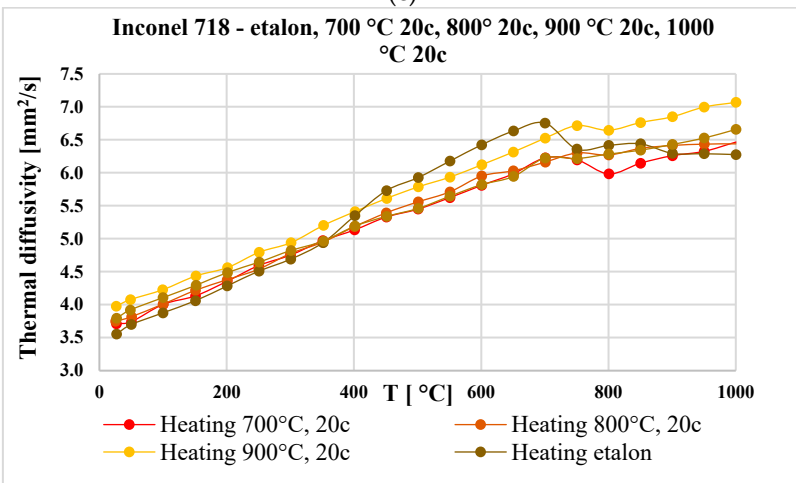

(**d**)

Figure 13. The variation in the thermal diffusivity of the samples subjected to the same number of thermal shocks depending on the shock threshold temperature: (**a**) 3 thermal shock cycles; (**b**) 9 thermal shock cycles; (**c**) 12 thermal shock cycles; (**d**) 20 thermal shock cycles.

The increase in the thermal diffusivity values of nickel-based superalloys in their as-delivered state with the measuring temperature was determined by A. Hazotte, B. Perrot, and P. Archambault [34] for single-crystal Ni-based superalloys, as well as by Zielinska [35]

and A. Sh. Agazhanov, D. A. Samoshkin, and Yu. M. Kozlovskii [36] for Inconel 718. In the evolution of the thermal diffusivity curve with the measuring temperature determined by Zielinska, an inflection point appears around 700 °C, while Hazotte and collaborators note a peak around this temperature. The research presented in this paper shows the maximum evolution at 700 °C for the Inconel alloy in its as-delivered state, as well as peaks at 700 °C and 900 °C for samples subjected to cyclic thermal shocks.

The present research reveals the influence of thermal shock temperature, as well as the number of shocks applied at the same temperature, on the evolution of thermal diffusivity curves with the measuring temperature.

3.2.2. The Influence of the Number of Cycles Applied at the Same Temperature

The variation in thermal diffusivity with an increasing number of thermal shock cycles applied at the same temperature, from 3 to 20, results in $\alpha = f(T)$ curves with similar profiles. For a large number of cycles, the diffusivity at high temperatures increases with the number of thermal shock cycles (Figure 14).

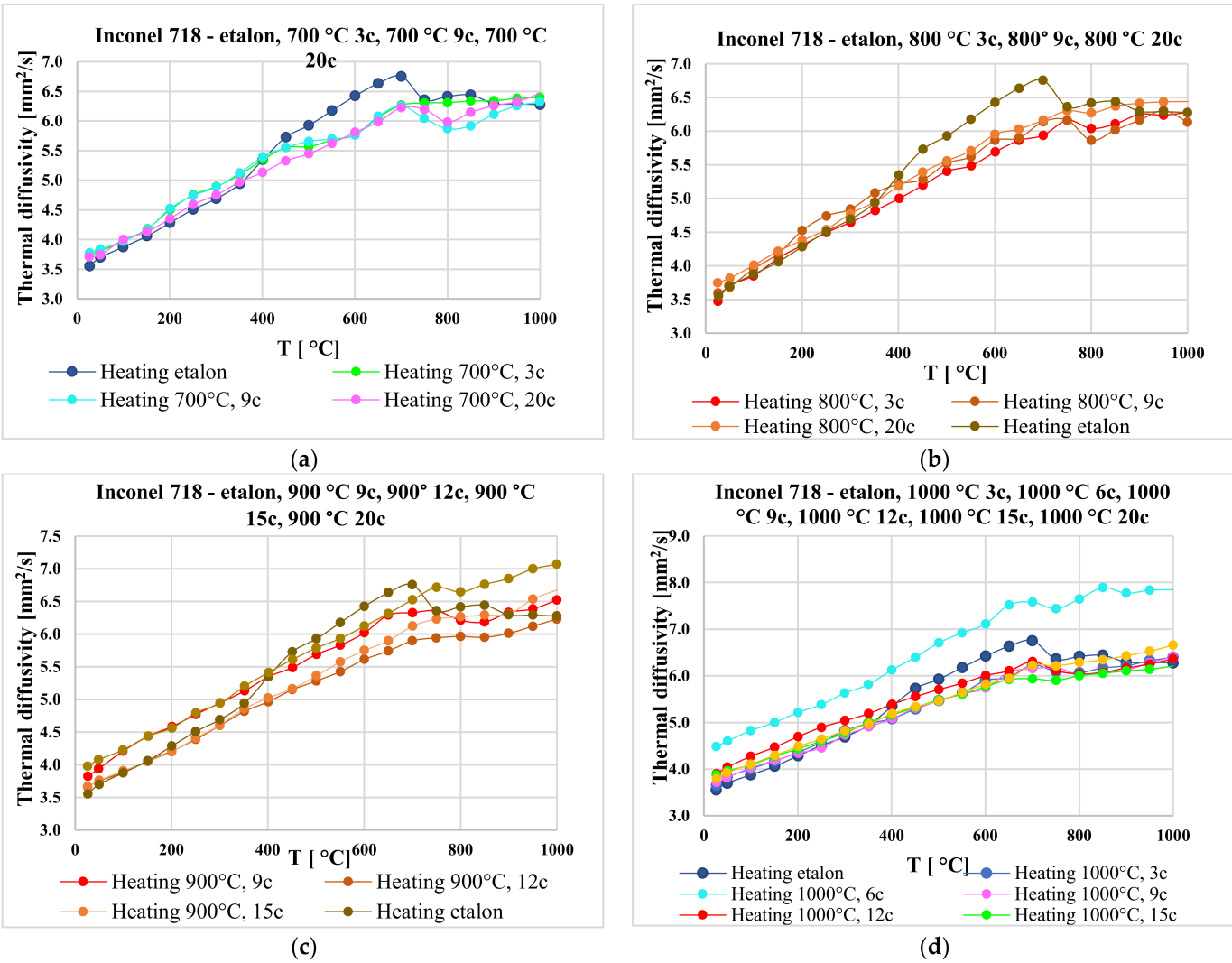

Figure 14. Variation in thermal diffusivity with the number of cycles applied to the following: (**a**) 700 °C; (**b**) 800 °C; (**c**) 900 °C; (**d**) 1000 °C.

3.3. The Effect of Cyclic Overheating on the Width of the Heat-Affected Zone

The size of the heat-affected zone (HAZ) due to overheating was assessed through hardness measurements. Hardness variations show decreasing curves from the surface opposite to the surface where the shocks were applied.

For the same number of thermal shocks applied, increasing the shock temperature results in a widening of the heat-affected zone (see Figure 15a,b). In the case of samples subjected to thermal shocks at 700 °C, a variation with a peak before a marked decrease is observed, a phenomenon that can be explained by an increase in the number of precipitates upon recovery.

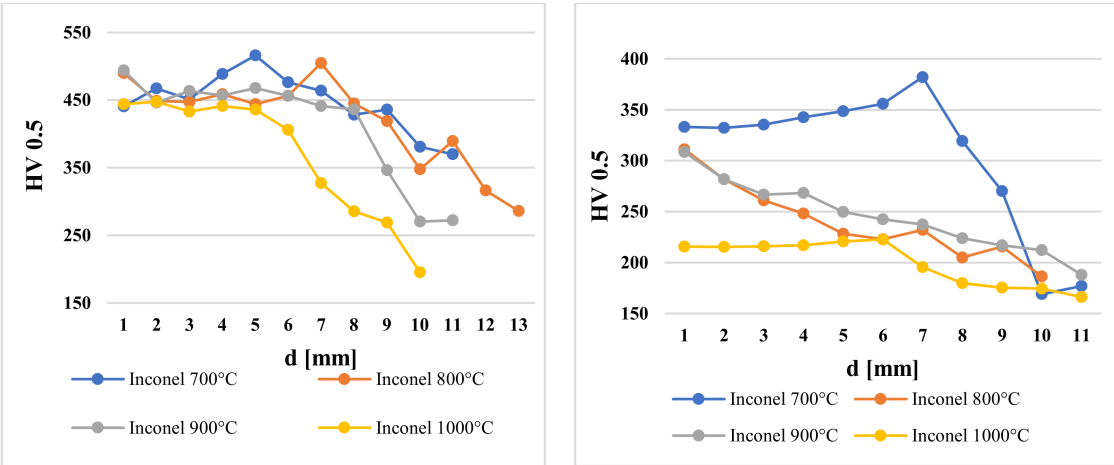

(**a**) (**b**)

Figure 15. The decrease in hardness near the shock surface as a function of the thermal shock temperature for the same number of applied thermal shock cycles: (**a**) 9 thermal cycles; (**b**) 20 thermal cycles; 'd'—the distance from the opposite surface to the thermal shocks' application surface.

Through microhardness measurements, this paper also presents the evolution of the thermally affected zone for the conditions of thermal shock application parameters.

An increase in the number of shocks applied at the same temperature leads to an expansion of the heat-affected zone (Figure 16a–d). For 20 cycles of overheating applied at 1000 °C, the hardness is less than half of the value in the as-delivered state.

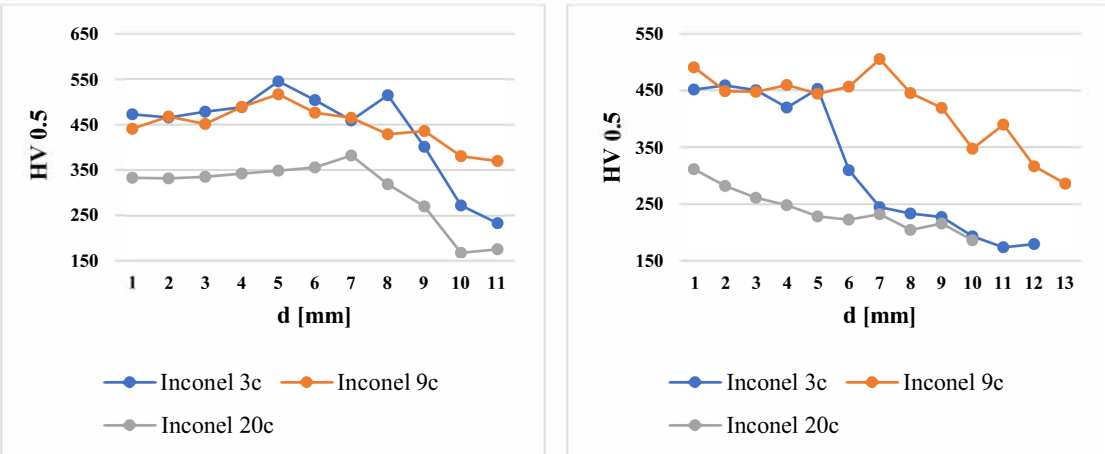

(**a**) (**b**)

Figure 16. *Cont.*

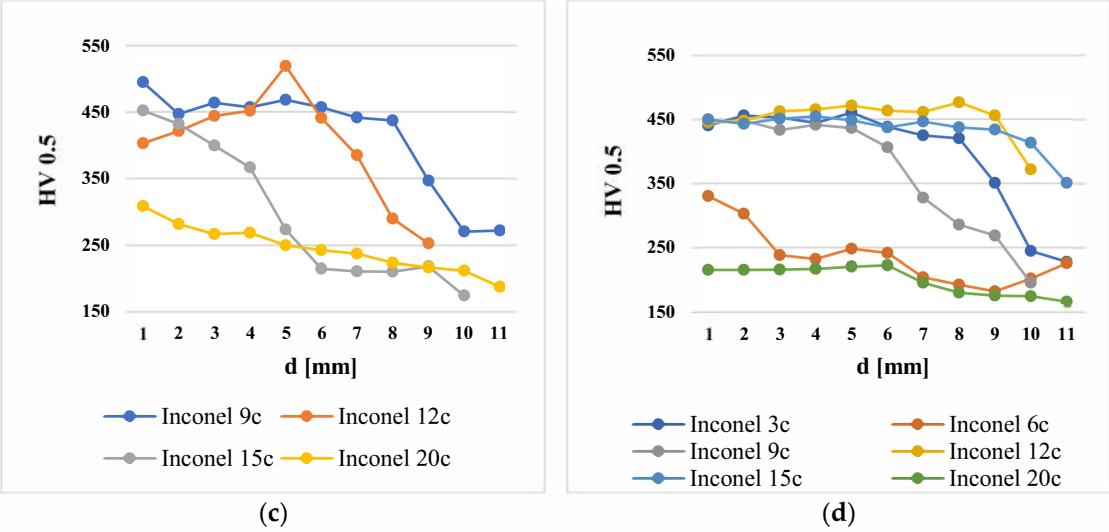

(**c**) (**d**)

Figure 16. The decrease in hardness relative to the thermal shock surface as a function of the number of cycles applied at the same temperature: (**a**) 700 °C; (**b**) 800 °C; (**c**) 900 °C; and (**d**) 1000 °C; 'd'—the distance from the opposite surface to the thermal shocks' application surface.

4. Conclusions

The results regarding the evolution of the microstructure and thermal transfer process in the Inconel 718 alloy subjected to short, repeated heating at high temperatures, up to 1000 °C, have been presented.

The reproduction of accidental, short-term increases in temperature was achieved by applying thermal shocks with solar energy for a history of 3 to 20 cycles.

The microstructural analysis of the samples treated by thermal shocks highlighted the distribution and size of the precipitates located at the grain boundaries and the large intragranular precipitates.

The SEM EDS characterization of the acicular γ'' precipitates showed a high niobium content, even up to 78.91% Nb, in accordance with studies conducted by Godka et al. [39,40].

The increase in the number of thermal cycles and the temperature of the shocks led to a decrease in the number of intragranular precipitates, an increase in the size of the remaining ones, and their arrangement in strings oriented perpendicular to the surface where the thermal shock was applied. At high temperatures, the acicular phases disappeared, and the structure remained polyhedral with fine intergranular precipitates.

The morphology and elemental chemical composition of the oxide layers were characterized. The layer formed at 800 °C was compact and exhibited a stratified distribution of the alloying elements, with a significant area rich in chromium near the oxide–metal interface. At 1000 °C, the oxide layer showed signs of degradation, with a less distinct distribution of elements, but maintained a thinner chromium-rich layer near the interface with the metal [41].

The oxide layer formed on the surface of the samples exhibited a stratified distribution of alloying elements in layers parallel to the metal–oxide interface. Notably, there was a chromium-rich layer in the immediate vicinity of the metal–oxide interface, with continuous and substantial thickness, which accounts for the high corrosion resistance.

Increasing the thermal shock application temperature for samples subjected to the same number of shocks highlighted an increase in diffusivity. For the same thermal shock temperature, increasing the number of applied shocks led to an increase in diffusivity.

The diffusivity values of the samples after being subjected to thermal shocks were close to and permanently lower than those recorded for the reference sample, except for one sample (1000 °C, six cycles).

The variation curve for the reference sample showed a maximum in the range of 600–750 °C (in accordance with studies conducted by Hazotte and Archambault) and a

small maximum below 850 °C. For the samples previously subjected to thermal shocks, these maxima were small.

Increasing the temperature for the same number of thermal shocks and increasing the number of shocks applied at the same temperature led to an increase in the depth of the heat-affected zone below the surface of shock application, reaching the full length of the sample for 20 cycles applied at 1000 °C.

The experimental results contribute to expanding the database for the Inconel 718 alloy. They are useful for evaluating the heating/cooling rates during heat treatment, assessing the mechanical properties of surfaces subjected to cyclic thermal stresses, and evaluating the depth affected by structural transformations. Future research aims to further study the variation with the maximum diffusivity curves and to conduct a similar study for other candidate alloys for Generation IV reactors.

Author Contributions: Conceptualization, M.A., E.R.U.A. and D.A.N.; methodology, E.R.U.A., A.G., D.A.N. and M.A.; software, D.A.N. and E.R.U.A.; validation, E.R.U.A., D.A.N. and M.A.; formal analysis, D.A.N.; investigation, E.R.U.A., D.A.N., A.G., M.G., D.-C.A., A.-D.R., A.I.J. and M.B.; resources, E.R.U.A.; data curation, M.I.P.; writing—original draft preparation, E.R.U.A. and M.A.; writing—review and editing and visualization, D.A.N. and M.I.P.; supervision, M.A. and D.-C.A.; project administration, M.A. All authors have read and agreed to the published version of the manuscript.

Funding: This project has received funding from the European Union's Horizon 2020 research and innovation programme under grant agreement No 823802. We thank the CNRS-PROMES laboratory, UPR 8521, belonging to the French National Centre for Scientific Research (CNRS) for providing access to its installations, the support of its scientific and technical staff, within this grant agreement No 823802 (SFERA-III).

Institutional Review Board Statement: Not applicable.

Informed Consent Statement: Not applicable.

Data Availability Statement: All data results are present in the present article.

Acknowledgments: We thank the team of the PROMES Laboratory, Font Romeu-Odeillo, especially our colleagues Anita Heussler and Emmanuel Guillot for their support in conducting thermal shock testing using solar energy, as part of the research carried out for the "Study of the variation of the mechanical properties of the superalloys Inconel 718 and Rene 41 under thermal shock—TERMOINCORENE".

Conflicts of Interest: The authors declare no conflicts of interest.

Abbreviations

SEM = Scanning Electron Microscopy; EDS = energy-dispersive spectroscopy; XRD = X-ray diffraction; HV = Vickers Hardness; cps: counts per second; $Ni_3(Al, Ti)$ = intermetallic compound; Ni_3Nb = intermetallic compound; Cr_2O_3 = Cr oxide; $Ti_{0.95}Nb_{0.95}O_4$ = titanium compound.

References

1. Alloy 718/Inconel 718 (W-Nr. 2.4668; UNS N07718). Available online: https://www.specialmetals.com (accessed on 10 June 2024).
2. Bhadeshia, H.K.D.H. Nickel Based Superalloys. Available online: https://www.phase-trans.msm.cam.ac.uk/2003/Superalloys/superalloys.html (accessed on 10 June 2024).
3. Pollock, T.M.; Tin, S. Nickel-Based Superalloys for Advanced Turbine Engines: Chemistry, Microstructure and Properties. *J. Propuls. Power* **2006**, *22*, 361–374. [CrossRef]
4. Maj, P.; Adamczyk-Cieslak, B.; Slesik, M.; Mizera, J.; Pieja, T.; Sieniawski, J.; Gancarczyk, T.; Dudek, S. The Precipitation Processes and Mechanical Properties of Aged Inconel 718 Alloy After Annealing. *Arch. Metall. Mater.* **2017**, *62*, 1695–1702. [CrossRef]
5. Wu, Y.; Zhao, H.; Li, J.; Zhang, Y.; Liu, J.; Liu, T. An innovative approach towards forming the serrated grain boundaries and refining the γ' precipitates in nickel-based superalloys. *J. Alloys Compd.* **2022**, *908*, 164570. [CrossRef]
6. Vincent, R. Precipitation around and welds in the nickel-base superalloy, Inconel 718. *Acta Metall.* **1985**, *33*, 1205–1216. [CrossRef]

7. Ranganath, S.; Guo, C.; Holt, S. Experimental Investigations into the Carbide Cracking Phenomenon on Inconel 718 Superalloy Material. In Proceedings of the ASME 2009 International Manufacturing Science and Engineering Conference, West Lafayette, IN, USA, 4–7 October 2009; pp. 33–39. [CrossRef]
8. Guan, H.; Jiang, W.; Lu, J.; Zhang, Y.; Zhang, Z. Precipitation of δ phase in Inconel 718 superalloy: The role of grain boundary and plastic deformation. *Mater. Today Commun.* **2023**, *36*, 106582. [CrossRef]
9. Feng, Q.; Wu, Y.; Li, J.; Cai, Y.; Zhang, Y.; Liu, J.; Liu, T. Effects of intermediate temperature on the grain boundary and γ' precipitates of nickel-based powder superalloy under interrupted cooling. *J. Alloys Compd.* **2022**, *922*, 166310. [CrossRef]
10. Huang, H.; Liu, G.; Wang, H.; Wang, Z.; Zhang, H.; Shao, Y.; Hu, B. Effect of cooling rate and resulting microstructure on tensile properties and deformation mechanisms of an advanced PM nickel-based superalloy. *J. Alloys Compd.* **2019**, *805*, 1254–1259. [CrossRef]
11. Mitchell, R.J.; Preuss, M.; Tin, S.; Hardy, M.C. The influence of cooling rate from temperatures above the γ' solvus on morphology, mismatch and hardness in advanced polycrystalline nickel-base superalloys. *Mater. Sci. Eng. A* **2008**, *473*, 158–165. [CrossRef]
12. Singh, A.R.P.; Nag, S.; Hwang, J.Y.; Viswanathan, G.B.; Tiley, J.; Srinivasan, R.; Fraser, H.L.; Banerjee, R. Influence of cooling rate on the development of multiple generations of γ' precipitates in a commercial nickel base superalloy. *Mater. Charact.* **2011**, *62*, 878–886. [CrossRef]
13. Babu, S.; Miller, M.K.; Vitek, J.M.; David, S.A. Characterization of the microstructure evolution in a nickel base superalloy during continuous cooling conditions. *Acta Mater.* **2001**, *49*, 4149–4160. [CrossRef]
14. Wu, H.; Li, J.; Liu, F.; Huang, L.; Zeng, X.; Fang, Q.; Huang, Z.; Jiang, L. A high-throughput methodology search for the optimum cooling rate in an advanced polycrystalline nickel base superalloy. *Mater. Des.* **2017**, *128*, 176–181. [CrossRef]
15. Osada, T.; Gu, Y.; Nagashima, N.; Yuan, Y.; Yokokawa, T.; Harada, H. Optimum microstructure combination for maximizing tensile strength in a polycrystalline superalloy with a two-phase structure. *Acta Mater.* **2013**, *61*, 1820–1829. [CrossRef]
16. Sarosi, P.M.; Wang, B.; Simmons, J.P.; Wang, Y.; Mills, M.J. Formation of multimodal size distributions of γ' in a nickel-base superalloy during interrupted continuous cooling. *Scr. Mater.* **2007**, *57*, 767–770. [CrossRef]
17. Chen, Y.; Yu, H.; Chen, Y.; Di, H.; Xu, W. The strengthening effects and mechanisms of alloying elements on interfaces for multiphase Ni-based superalloys: A first-principles study. *J. Mater. Res. Technol.* **2023**, *23*, 4802–4813. [CrossRef]
18. Zhao, S.; Xie, X.; Smith, G.D.; Patel, S.J. Gamma prime coarsening and age-hardening behaviors in a new nickel base superalloy. *Mater. Lett.* **2004**, *58*, 1784–1787. [CrossRef]
19. Grosdidier, T.; Hazotte, A.; Simon, A. Precipitation and dissolution processes in γ/γ' single crystal nickel-based superalloys. *Mater. Sci. Eng. A-Struct. Mater. Prop. Microstruct. Process.* **1998**, *256*, 183–196. [CrossRef]
20. Guo, X.; He, H.; Chen, F.; Liu, J.; Zhao, H. Microstructural Degradation and Creep Property Damage of a Second-Generation Single Crystal Superalloy Caused by High Temperature Overheating. *Materials* **2023**, *16*, 1682. [CrossRef]
21. Jiang, W.; Lu, J.; Guan, H.; Wang, M.; Cheng, X.; Li, L.; Liu, X.; Wang, J.; Zhang, Y.; Zhan, Z.; et al. Study of pre-precipitated δ phase promoting deformation twinning and recrystallization behavior of Inconel 718. *Mater. Des.* **2023**, *226*, 111693. [CrossRef]
22. Glotka, O. Distribution of Alloying Elements in Carbides of Refractory Nickel Alloys under the Conditions of Equiaxial Crystallization. *Mater. Sci.* **2021**, *56*, 714–721. [CrossRef]
23. Nunes, R.M.; Pereira, D.; Clarke, T.; Hirsch, T.K. Delta Phase Characterization in Inconel 718 Alloys Through X-ray Diffraction. *ISIJ Int.* **2015**, *55*, 2450–2454. [CrossRef]
24. Tucho, W.M.; Ohm, B.A.; Canizalez, S.A.P.; Egeland, A.; Mildt, M.B.; Nedreberg, M.L.; Hansen, V.F. Efects of δ Phase and Annealing Twins on Mechanical Properties and Impact Toughness of L-PBF Inconel 718. *J. Manuf. Mater. Process.* **2024**, *8*, 135. [CrossRef]
25. Lee, J.L.; Wang, P.T.; Lo, K.C.; Shen, P.K.; Tsou, N.T.; Kakehi, K.; Murakami, H.; Tsai, C.W.; Gorsse, S.; Yeh, A.C. Effect of serrated grain boundary on tensile and creep properties of a precipitation strengthened high entropy alloy. *Sci Technol Adv Mater.* **2023**, *24*, 2158043. [CrossRef] [PubMed]
26. Oros, T.J.; Son, K.; Hodge, A.M.; Kassner, M.E. The high temperature creep and fracture behavior of Inconel 718 produced by additive manufacturing. *Scr. Mater.* **2024**, *251*, 116208. [CrossRef]
27. Wang, S.L.; Sun, Y.R.; Du, L.J.; Liu, L.; Wang, J.; Xiang, D.H. Influence of thermal shock behavior on microstructure and mechanical properties of IN718 superalloy. *Appl. Surf. Sci.* **2019**, *484*, 1282–1287. [CrossRef]
28. Vulpe, S.C.; Abrudeanu, M.; Ohai, D.; Plaiasu, A.G.; Radutoiu, N. The Influence of the Thermal Cycling on Grains Size of the Nickel-based Alloys. *Rev. Chim.* **2012**, *63*, 1112–1115.
29. Vulpe, S.C.; Abrudeanu, M.; Ohai, D.; Plaiasu, A.G.; Rizea, V.; Radutoiu, N. The Influence of the Thermal Transient Regime on Grain Size at Nickel-based Alloys. *Rev. Chim.* **2022**, *63*, 1026–1030.
30. Mukhopadhyay, S.; Sriram, H.; Zenk, C.H.; DiDomizio, R.; Detor, A.J.; Hayes, R.W.; Viswanathan, G.B.; Wang, Y.; Mills, M.J. Creep Behavior of Compact γ'-γ'' Coprecipitation Strengthened IN718-Variant Superalloy. *Metals* **2021**, *11*, 1897. [CrossRef]
31. Shi, R.; McAllister, D.P.; Zhou, N.; Detor, A.J.; DiDomizio, R.; Mills, M.J.; Wang, Y. Growth behavior of γ'/γ'' coprecipitates in Ni-Base superalloys. *Acta Mater.* **2019**, *164*, 220–236. [CrossRef]
32. Thornton, E.-L.; Zannoun, H.; Vomero, C.; Caudill, D.; Schoop, J. A Review of Constitutive Models and Thermal Properties for Nickel-Based Superalloys Across Machining-Specific Regimes. *J. Manuf. Sci. Eng.* **2023**, *145*, 080801. [CrossRef]
33. Miura, A.; Osada, T.; Kawagishi, K.; Uchida, K.-I. Thermal transport properties of Ni–Co-based superalloy. *AIP Adv.* **2020**, *10*, 125118. [CrossRef]

34. Hazotte, A.; Perrot, B.; Archambault, P. High temperature thermal diffusivity of nickel-based superalloys and intermetallic compounds. *Le J. De Phys. IV* **1993**, *3*, C7-351–C7-354. [CrossRef]
35. Zieliñska, M.; Yavorska, M.; Porêba, M.; Sieniawski, J. Thermatl propreties of cast nickel-based alloys. *Arch. Mater. Sci. Eng.* **2010**, *44*, 35–38.
36. Agazhanov, A.S.; Samoshkin, D.A.; Kozlovskii, Y.M. Thermophysical properties of Inconel 718 alloy. *J. Phys. Conf. Ser.* **2019**, *1382*, 012175. [CrossRef]
37. Glotka, A.A.; Haiduk, S.V.; Ol'shanetskii, V.Y. Modeling Thermophysical Characteristics of Nickel-Based Superalloys. *J. Eng. Phys. Thermophy* **2021**, *94*, 1363–1368. [CrossRef]
38. *ASTM B637 N07718*; Standard Specification for Nickel Alloy Bars, Forgings, and Forging Stock for Moderate or High Temperature Service. ASTM: West Conshohocken, PA, USA, 2023.
39. Glotka, A.; Ol'shanetskii, V. Influence of alloying systems on the properties of single crystal nickel-based superalloy. *Int. J. Mater. Res.* **2021**, *112*, 794–799. [CrossRef]
40. Zhang, Y.; Qin, L.; Zhu, B.; Jiang, H.; Tan, L.; Huang, T.; Gan, B.; Jie, Z.; Liu, L. Optimizing a Solution Heat Treatment by Increasing the Cooling Rate of Directional Solidification for Ni-Based Superalloys. *Materials* **2023**, *16*, 3433. [CrossRef]
41. Rucai, V.; Constantin, N.; Dobrescu, C. Experimental Research Program Regarding the Influence of Thermo-Time Treatment of Multicomponent Ni-Base Melting on Their Properties in Solid Phase. *U.P.B. Sci. Bull. Ser. B Vol.* **2015**, *77*, 359–363.